

Site occupation of Al doping in $Lu_{2s}iO_5$: The role of ionic radius versus chemical valence

Xuejiao Sun(孙雪娇), Yu Cui(崔宇), Feng Gao(高峰), Zhongjun Xue(薛中军), Shuwen Zhao(赵书文), Dongzhou Ding(丁栋舟), Fan Yang(杨帆), and Yi-Yang Sun(孙宜阳)

Citatio: Chin. Phys. B, 2025, 34 (**9**): 096101. DOI: 10.1088/1674-1056/add678
http://cpb.iphy.ac.cn; http://iopscience.iop.org/cpb

What follows is a list of articles you may be interested in

General-purpose moment tensor potential for Ga-In liquid alloys towards large-scale molecular dynamics with *ab initio* accuracy

Kai-Jie Zhao(赵凯杰) and Zhi-Gong Song(宋智功)

Chin. Phys. B, 2025, 34 (**6**): 066101. DOI: 10.1088/1674-1056/adc661

Effect of copper/tungsten heterophase interface on radiation resistance: Insights from atomistic simulations

Wen Chen(陈文), Min Li(李敏), Bao-Qin Fu(付宝勤), Tun Chen(陈暾), Jie-Chao Cui(崔节超), and Qing Hou(侯氢)

Chin. Phys. B, 2025, 34 (**4**): 046108. DOI: 10.1088/1674-1056/adb40d

Non-negligible influence of vacancies and interlayer coupling on electronic properties of heavy ion irradiated $SnSe_2$ FETs

Shifan Gao(高诗凡), Siyuan Ma(马思远), Shengxia Zhang(张胜霞), Pengliang Zhu(朱彭靓), Jie Liu(刘杰), Lijun Xu(徐丽君), Pengfei Zhai(翟鹏飞), Peipei Hu(胡培培), and Yan Li(李燕)

Chin. Phys. B, 2025, 34 (**4**): 046106. DOI: 10.1088/1674-1056/adb270

Visualizing extended defects at the atomic level in a $Bi_2Sr_2CaCu_2O_{8+\delta}$ superconducting wire

Kejun Hu(胡柯钧), Shuai Wang(王帅), Boyu Li(李泊玉), Ying Liu(刘影), Binghui Ge(葛炳辉), and Dongsheng Song(宋东升)

Chin. Phys. B, 2024, 33 (**9**): 096101. DOI: 10.1088/1674-1056/ad6ccd

Properties of radiation defects and threshold energy of displacement in zirconium hydride obtained by new deep-learning potential

Xi Wang(王玺), Meng Tang(唐孟), Ming-Xuan Jiang(蒋明璇), Yang-Chun Chen(陈阳春), Zhi-Xiao Liu(刘智骁), and Hui-Qiu Deng(邓辉球)

Chin. Phys. B, 2024, 33 (**7**): 076103. DOI: 10.1088/1674-1056/ad362b

---

Site occupation of Al doping in Lu_2SiO_5: The role of ionic radius versus chemical valence

Xuejiao Sun(孙雪娇)[1,2], Yu Cui(崔宇)[1,2], Feng Gao(高峰)[1,†], Zhongjun Xue(薛中军)[2], Shuwen Zhao(赵书文)[2], Dongzhou Ding(丁栋舟)[2], Fan Yang(杨帆)[3], and Yi-Yang Sun(孙宜阳)[2,‡]

[1] *School of Physics, Changchun Normal University, Changchun* 130032, *China*
[2] *State Key Laboratory of High Performance Ceramics and Superfine Microstructure, Shanghai Institute of Ceramics, Chinese Academy of Sciences, Shanghai* 201899, *China*
[3] *Key Laboratory of Weak-Light Nonlinear Photonics, Ministry of Education, School of Physics, Nankai University, Tianjin* 300071, *China*

(Received 12 January 2025; revised manuscript received 8 April 2025; accepted manuscript online 9 May 2025)

Lu_2SiO_5:Ce (LSO:Ce) serving as a core material for radiation detectors, plays a crucial role in the design and development of positron emission tomography (PET) devices. Experiment has confirmed that low concentration of Al doping can significantly enhance the light yield, decay time, rise time, energy resolution, and afterglow level of the LSO:Ce crystals. The mechanisms regarding the lattice site occupancy of Al in LSO, while closely associated with the performance improvements, are not yet fully understood. Particularly, it is unclear either the ionic radius or the chemical valence plays a more critical role in determining the site occupancy. In this study, we utilized first-principles calculations based on density functional theory (DFT) to study the lattice site occupancy of Al in LSO crystals and to explore their impact on the electronic structure. Our results indicate that with changes in the growth environment, as reflected by the atomic chemical potentials, Al can occupy either the Si sites or the Lu_2 sites, and it is not inclined to occupy the Lu_1 sites. The doping of Al at the Si site introduces a shallow acceptor level, which may contribute to the suppression of trap concentration and affect the ratio of Ce^{3+} to Ce^{4+} within the crystal, thereby influencing its scintillation properties.

Keywords: sincitillation materials, silicates, defects, first-principles calculations

PACS: 61.72.–y, 31.15.es, 29.40.Mc

DOI: 10.1088/1674-1056/add678 **CSTR:** 32038.14.CPB.add678

1. Introduction

Since the introduction of cerium-doped lutetium oxyorthosilicate (Lu_2SiO_5:Ce or LSO:Ce) in the early 1990s, it has shown broad application prospects in various fields such as medical imaging, high-energy physics experiments, and geophysical exploration, due to its high density (7.4 g/cm^3), high light yield (3×10^4 photons/MeV), and fast decay time (40 ns).[1] Especially in the field of nuclear medical imaging, LSO:Ce has been widely applied in positron emission tomography (PET) and x-ray computed tomography (CT).[2,3] As the core material of PET detectors,[4] scintillation crystals play an essential role in improving image quality and efficiency. With the advancement of time-of-flight positron emission tomography (TOF-PET) technology, there is an increased demand for scintillation crystals with higher time resolution and high light yield.[5,6] To enhance image quality, reduce image acquisition time, and further achieve application in medical imaging devices with full-body scanning capabilities, the key lies in improving the performance of LSO crystals.

Element substitution and co-doping of cations have been demonstrated to be effective methods for improving the performance of scintillators.[7] LSO and Y_2SiO_5 (YSO) form an infinite solid solution system,[8] and the introduction of yttrium ions not only lowers the melting point of the material, but also increases its light yield.[9] The typical method of co-doping involves partially replacing rare-earth ions with divalent cations such as Ca^{2+} (Ref. [10]) and Mg^{2+} (Ref. [11]), which suppress electron trapping and stabilizes the formation of Ce^{4+}, thus significantly enhancing the scintillation light yield and reducing the decay time.[11–14] The presence of Ce^{4+} bypasses the initial hole capture process of Ce^{3+} emission, effectively enhancing the efficiency of the scintillation light emission. In the $(Lu,Y)_2SiO_5$:Ce (LYSO:Ce) system, co-doping with Ca^{2+} is widely considered to be the state of the art with the best performance. In 2023, experiments successfully achieved the doping of Al in LYSO:Ce crystals and grew crystals with various Al concentrations.[15] When the doping concentration of Al reached 0.6 atomic percent, the scintillation performance of the crystals was significantly enhanced. Compared to undoped crystals, the signal-to-noise ratio has been improved by 1.4 times, which is beneficial for the development of next-generation TOF-PET technology. Moreover, the performance of the afterglow level and energy resolution is superior to that of Ca^{2+} co-doping.[16]

†Corresponding author. E-mail: 5234110@qq.com
‡Corresponding author. E-mail: yysun@mail.sic.ac.cn

© 2025 Chinese Physical Society and IOP Publishing Ltd. All rights, including for text and data mining, AI training, and similar technologies, are reserved.

To understand the high performance of Al-doped LSO:Ce, it is imperative to know the site of Al atoms in the crystal structure. The ability of an element to be doped into a host material is closely related to the ionic radius and chemical valence of the dopant element. Generally, the closer the radius of the dopant ion is to the replaced host ion and the smaller the difference in their chemical valences, the easier the doping process will be. Although Al^{3+} (with an ionic radius of 0.39 Å) and Lu^{3+} (with an ionic radius of 0.86 Å) have the same chemical valence, their ionic radii differ significantly. In contrast, Al^{3+} and Si^{4+} (with an ionic radius of 0.26 Å) have relatively smaller difference in ionic radius, but their chemical valences are different.[17] It is thus not certain that Al prefers to occupy Lu or Si site. In addition, there are two Lu sites in this crystal, there site occupancy is also worth of study. In this work, we use first-principles calculations to investigate the stability of Al in LSO crystals, aiming to provide references and guidance for the doping engineering of the LSO crystal.

2. Computational method

This study employs the first-principles calculations based on density functional theory (DFT) as implemented in the Vienna *ab initio* simulation package (VASP).[18] The interactions between ion-cores and valence electrons were described by the projector augmented wave (PAW) method.[19,20] We performed calculations using the Perdew–Burke–Ernzerhof for solids (PBEsol) functional within the generalized gradient approximation (GGA)[21] and the Heyd–Scuseria–Ernzerhof (HSE06) hybrid exchange–correlation functional.[22] The supercell method was used to model the defects. A 128-atom supercell was used and the Γ-point was used to represent the Brillouin zone of the supercell. All calculations on neutral defects, which exhibit a spin magnetic moment of 1 μ_B, were spin-polarized. The atomic structures were fully relaxed until the calculated forces on all atoms were less than 0.025 eV/Å. Plane waves with cutoff energy of at least 400 eV were taken as the basis set. When calculating the atomic chemical potentials, the product of the k-point numbers and the lattice constants along the three lattice vectors was approximately 20 Å. The setup above yielded $a = 14.285$ Å, $b = 6.632$ Å, $c = 10.198$ Å, and $\beta = 122.2°$ for LSO.

Defect formation energy is a function of atomic chemical potential and Fermi level. The formation energy of a point defect carrying a charge q was calculated as follows:[23,24]

$$\Delta H(\mu_i, E_F, q) = E_D^q - E_P + \sum_i n_i(\mu_i^* + E_i) + q(E_F + E_{VBM}),$$

where E_D^q is the total energy of the supercell containing a point defect of charge q, E_P is the total energy of the perfect supercell, n_i is the number of atoms added (n_i<0) or removed (n_i>0) from the supercell during the formation of the defects, μ_i^* is the chemical potential of the constituent element i, E_i is the total energy of each atom in its stable phase. The allowable range for μ_i^* is determined by the presence of various secondary phases. E_{VBM} represents the energy of the valence band maximum (VBM) of the host material, while E_F denotes the Fermi level, which varies between the VBM and the conduction band minimum (CBM). Defect transition level refers to the Fermi level when a defect has the same formation energy in different charge states. For a defect with its transition from charge state q to q', the defect transition level can be expressed as[25]

$$\varepsilon(q/q') = \left(\frac{E_D^q - E_D^{q'}}{q' - q}\right) - E_{VBM}.$$

To determine the allowable range of chemical potentials for LSO, the chemical potentials need to satisfy

$$\begin{aligned}
&\mu_i^* \le 0 \quad \text{for all elements},\\
&2\mu_{Lu}^* + \mu_{Si}^* + 5\mu_O^* = \Delta H_{Lu_2SiO_5} = -27.41 \text{ eV},\\
&2\mu_{Lu}^* + 3\mu_O^* \le \Delta H_{Lu_2O_3} = -18.59 \text{ eV},\\
&\mu_{Si}^* + 2\mu_O^* \le \Delta H_{SiO_2} = -8.65 \text{ eV},\\
&2\mu_{Lu}^* + 2\mu_{Si}^* + 7\mu_O^* \le \Delta H_{Lu_2Si_2O_7} = -36.36 \text{ eV}
\end{aligned}$$

with ΔH representing the enthalpy of formation. For Al doping, additional conditions need to be satisfied, *i.e.*, ensuring thermodynamic stability of the LSO crystal by preventing the formation of other compounds between Al and the host elements, which will be further described below.

3. Results and discussion

As shown in Fig. 1(a), the 128-atom supercell is made of two unit cells. There are two different Lu sites, named Lu_1 and Lu_2, which are surrounded by seven and six O atoms with average Lu–O bond lengths of 2.31 Å and 2.22 Å, respectively. Si atoms occupy a single lattice site, located at the center of the [SiO_4] tetrahedron, with an average Si–O bond length of 1.64 Å. There are five types of O sites in LSO, four of them are bonded to Si atoms, while the remaining one is bonded only to Lu atoms. In this study, we considered Al to replace both Lu and Si sites. Our calculation shows that when Al replaces the Lu_1 site, one Al–O bond length increases significantly from 2.58 Å to 3.25 Å, as shown in Fig. 1(b). This change may stem from the smaller ionic radius and electronic configuration of Al, which favor a 6-coordinate structure over a 7-coordinate one to enhance the stability. This change in the coordination structure effectively leads to the breaking (or significant elongation) of the Al–O bond.

We computed the atomic chemical potentials and defect formation energies using the PBEsol and HSE06 functionals. During the doping process, the secondary phases formed by the interaction between dopant atoms and host atoms can influence the defect formation energy, which in turn affects the

doping limit.[26,27] We therefore determined the chemical potentials associated with the defect formation energy in Al-doped LSO. In Fig. 2(a), the equilateral triangle defines the chemical potential space spanned by μ^*_{Lu}, μ^*_{Si}, and μ^*_O that permit the formation of the primary phase, *i.e.*, LSO. During the synthesis of LSO, elements such as Lu, Si, and O are prone to form secondary phases like SiO_2, Lu_2O_3, and $Lu_2Si_2O_7$, which limit the allowable region for the chemical potentials. When using the PBEsol functional, the thermodynamically stable region of LSO is delineated by two dashed lines (blue and green), which correspond to SiO_2 and Lu_2O_3, respectively. Due to the relatively small formation enthalpies of LSO from the two secondary phases (about 0.17 eV per formula unit), the allowable region for the chemical potentials can be approximately represented with a red solid line AB, as shown in Fig. 2(a), which corresponds to the midpoint line of the narrow region. At the point A, $\mu^*_O = 0$, $\mu^*_{Lu} = -9.34$ eV, $\mu^*_{Si} = -8.74$ eV, and at the point B, $\mu^*_{Si} = 0$, $\mu^*_{Lu} = -2.78$ eV, $\mu^*_O = -4.37$ eV. When using the HSE06 functional, the thermodynamically stable region of LSO is delineated by SiO_2 and $Lu_2Si_2O_7$ (blue and orange). The formation enthalpies of LSO from these two secondary phases are approximately 0.35 eV per formula unit, as shown in Fig. 2(d). Nevertheless, the allowed chemical potentials are still limited in a narrow region, which can also be approximately represented by an AB line similar to that in Fig. 2(a). At the point A, $\mu^*_O = 0$, $\mu^*_{Lu} = -9.52$ eV, $\mu^*_{Si} = -9.07$ eV, and at the point B, $\mu^*_{Si} = 0$, $\mu^*_{Lu} = -2.72$ eV, $\mu^*_O = -4.54$ eV.

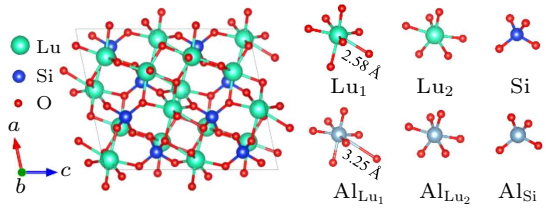


Fig. 1. (a) Crystal structure of Lu_2SiO_5 (LSO). Lu, Si, and O atoms are represented by blue, green, and red colors, respectively. (b) Local coordination structures of the LSO crystal before and after Al doping, which favor a 6-coordinate structure over a 7-coordinate one to enhance the stability. This change in the coordination structure effectively leads to the breaking (or significant elongation) of the Al–O bond, illustrating the structural changes due to Al substitution. Lu atoms are located at two distinct lattice sites, labeled as Lu_1 and Lu_2, respectively, each coordinated by seven and six O atoms. Si atoms are located at the centers of $[SiO_4]$ tetrahedra.

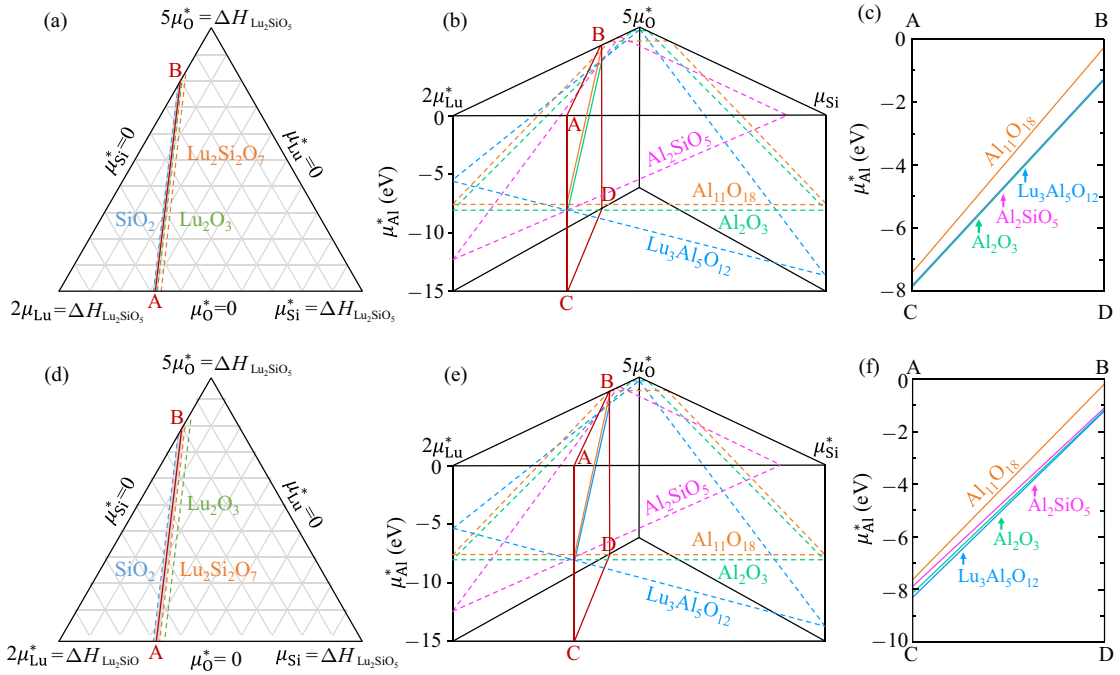


Fig. 2. Chemical potential analysis for the Lu–Si–O system with Al doping using PBEsol (top panels) and HSE06 (bottom panels) functionals. (a) Lu–Si–O system with allowed region between SiO_2 and Lu_2O_3. Red line AB shows the approximate allowed region. (b) Consider the dopant element Al, limited by the compounds formed between Al and the three primary elements, including $Al_{11}O_{18}$, $Lu_3Al_5O_{12}$, Al_2SiO_5, and Al_2O_3. (c) Allowed region of chemical potentials for Al-doped LSO. The formation of Al_2O_3 limits the system to achieve extreme Al-rich condition (*i.e.*, $\mu^*_{Al} = 0$). (d)–(f) Similar results obtained using the HSE06 functional.

O-rich ($\mu^*_O = 0$) or Si-rich ($\mu^*_{Si} = 0$) conditions are defined as the conditions where the chemical potential of O atoms or Si atoms reaches their respective maximum allowed values, A and B points, respectively. Under these conditions, we further considered the allowed range of the chemical potential for Al (μ^*_{Al}). As a dopant, it is desired that $\mu^*_{Al} = 0$, *i.e.*, the extreme Al-rich condition. However, it is actually limited by the formation of other Al-containing compounds. As shown in Fig. 2(b), the height of the triangular prism corresponds to the value of μ^*_{Al}. We calculated the formation enthalpies of all possible secondary phases that could be formed between Al and the host elements. Some of these secondary phases, such

as $LuAl_3$, $LuAl_2$, Lu_3Al_2, LuAl, LuAlSi, and Lu_2AlSi_2, do not significantly affect the favorable growth conditions of LSO and are not shown in the figure. In Figs. 2(b) and 2(e), only the secondary phases that limit μ^*_{Al} are presented, including $Al_{11}O_{18}$, Al_2SiO_5, Al_2O_3, and $Lu_3Al_5O_{12}$. The stable regions for these secondary phases intersect with the region of ABCD.

Based on the process above, we determined the thermodynamically stable range of chemical potentials for Al-doped LSO. As mentioned above, for each secondary phase, the sum of the chemical potentials of the constituent elements μ^*_i must be less than the formation enthalpy of that phase. Using the PBEsol functional, as depicted in Fig. 2(c), among these secondary phases, the oxide Al_2O_3 played a key role in preventing the growth condition reaching $\mu^*_{Al} = 0$, even though other secondary phases $Al_{11}O_{18}$, Al_2SiO_5, and $Lu_3Al_5O_{12}$ could also limit μ^*_{Al}. Specifically, only under Si-rich conditions, μ^*_{Al} could reach as high as -1.24 eV, whereas under the O-rich conditions, μ^*_{Al} can only be below -8.04 eV. Using the HSE06 functional, as depicted in Fig. 2(f), the oxide $Lu_3Al_5O_{12}$ plays the role in preventing the growth condition from reaching $\mu^*_{Al} = 0$. In other words, if one expects that Al can be doped in high concentration, the Si-rich (or relatively O-poor) condition will be required. Unfortunately, it is usually hard to be achieved, given the typical oxygen environment employed in the growth of LSO.

Figure 3 presents the band structure of LSO calculated using the PBEsol functional, which confirms the direct bandgap nature of the material at the Γ point. Based on this finding, a Γ-only k-point mesh was employed for defect calculations in Al-doped LSO. While the PBEsol calculation yields a band gap of 4.35 eV, the HSE06 calculations give an improved value of 6.27 eV, showing better agreement with experimental measurements (6.4 eV–6.6 eV).[28–30] Because of the high computational cost, we did not calculate the full band strcutre using the HSE06 functional.

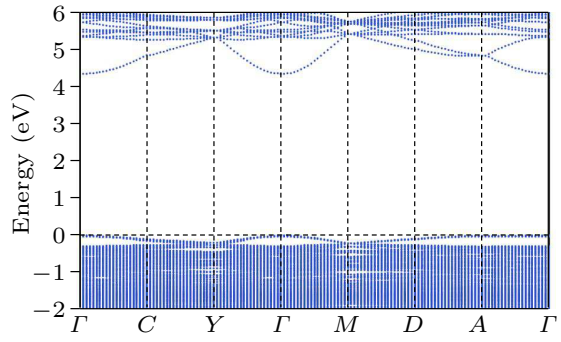


Fig. 3. Band structure of LSO using the PBEsol functional, with the top of the valence band set at zero.

Figure 4(a) shows the defect formation energies of Al at Lu and Si sites as a function of Fermi energy using the PBEsol functional. In the O-rich environment (left panels), when the Fermi level is above 1.1 eV, the lowest formation energy shifts from Al at the Lu_2 site to the Si site. In the Si-rich environment (right panel), this transition occurs at 3.28 eV. Using the HSE06 functional, the transitions are observed at 2.13 eV in the O-rich and 4.40 eV in the Si-rich environment. This difference is attributed to the well-known bandgap error of the semi-local functionals, such as PBEsol. In these calculations, we considered both $+1$ and -1 charge states. For Al on Si site, our results show that it is a shallow acceptor in PBEsol calculations, while the $(0/-)$ transition level is relatively deep in HSE06 calculations. For Al on Lu sites, PBEsol calculations did not yield transition level in the band gap, while HSE06 suggests a very deep donor level. In addition, the formation energy of Al at the Lu_1 site is consistently higher than that at the Lu_2 site, which is consistent with the observation that at Lu_1 site bond breaking is needed to accommodate the Al atom.

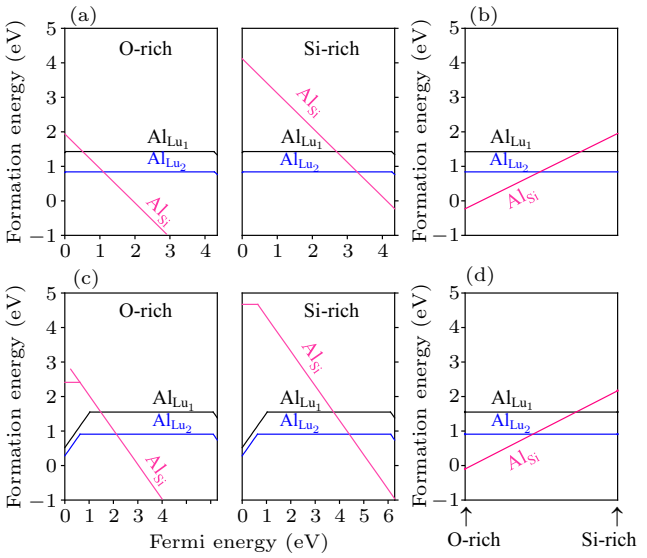


Fig. 4. Defect formation energy for Al doping of LSO as a function of Fermi energy (a) and chemical potentials (b) using the PBEsol functional. Panels (c) and (d) are obtained using the HSE06 functional. We considered Al on Lu (Lu_1 and Lu_2) sites and Si sites. The Fermi level varies between the VBM and CBM. When plotting panels (b) and (d), we set the Fermi level at the center of the band gap.

For undoped semiconductor materials, the Fermi level is typically located in the middle of the band gap. When the Fermi level is at the center of the band gap (3.14 eV), the defect formation energy is a function of the atomic chemical potentials. The relationship between defect concentration in a material and the defect formation energy as well as temperature can be described by

$$N_D = N_{site} \exp\left(-\frac{\Delta H}{k_B T}\right).$$

Here, N_{site} denotes the total number of lattice sites available for accommodating the defects or dopants, and T is taken as the experimental temperature for growing the crystal, which was taken to be 2150 °C. As shown in Fig. 4(d), in the O-rich environment, Al on Si site is more stable that Al on Lu sites. Note that the extreme O-rich condition cannot be reached, as the formation energy of Al on Si site becomes negative. As the

environment transitions from O-rich to Si-rich, the preference of Al shifts from the Si site to the Lu_2 site, where the formation energy is about 0.91 eV, resulting in a maximum doping concentration of about 1.3%. The experimental result shows that Al^{3+} codoping in LSO:Ce can reach 1%,[15] suggesting that the experimental grow condition is close to the transition point from Al_{Si} to Al_{Lu_2}. In this regard, the PBEsol results are consistent with the HSE06 results.

An interesting observation in Fig. 4 is that Al on Lu site is not dependent on the chemical potential. This is because the chemical potentials of Al and Lu change in the same trends. As can be seen in Fig. 2(c), from O-rich (A point) to Si-rich (B point) condition, μ^*_{Lu} increases from −9.34 eV to −2.78 eV, while μ^*_{Al} also increases from −7.87 eV to −1.32 eV. In Fig. 2(f), μ^*_{Lu} increases from −9.52 eV to −2.72 eV, while μ^*_{Al} also increases from −8.04 eV to −1.24 eV. Considering the equation of defect formation energy introduced in Section 2, the chemical potential dependence canceled each other, resulting in the observation that defect formation energy of Al on Lu is independent of the growth condition.

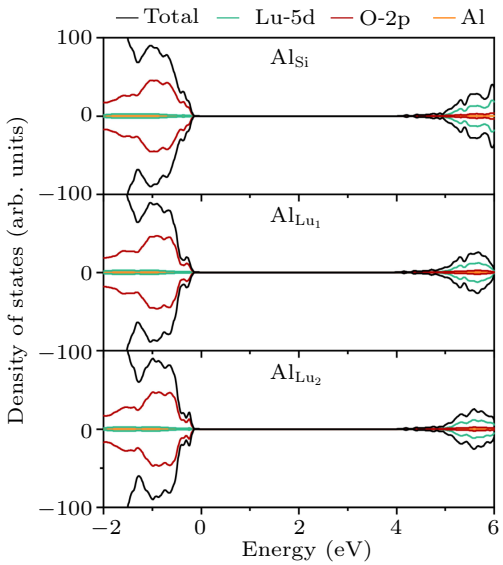


Fig. 5. Total and projected density of states for Al-doped LSO.

Figure 5 depicts the total and atomic projected density of states (DOS) of Al-doped LSO calculated at the neutral charge state. The projected DOS indicates that the VBM primarily consists of O-2p orbitals, while the CBM is mainly constituted by Lu-5d orbitals. In the case of Al on Si site, the defect energy level is at the VBM, *i.e.*, there is a hole at the VBM, resulting in minimal perturbation to the overall electronic structure of the host. This is consistent with the calculated shallow acceptor level in Fig. 4(a). Al on Lu sites yields clear band gaps with no any defect levels inside. Even though structurally there exists a difference between the two sites, as seen in Fig. 1, the electronic structures for Al on the two sites show negligible difference. The DOS calculations are also consistent with the observation that Al on Lu sites is free of defect transition levels as seen in Fig. 4.

Experimentally, to suppress O vacancy defects, supplementing oxygen during growth or oxidizing post-annealing after growth are commonly employed.[31,32] Such conditions are supposed to be O-rich, in which Al would tend to replace Si sites. The acceptors thus formed may compensate the O vacancies or oxidizing the Ce^{3+} to Ce^{4+} ions. The x-ray absorption near edge spectroscopy (XANES) spectra presented by Melcher *et al.* of LSO:Ce evidences that non-co-doped LSO crystals do not contain any Ce^{4+}.[33] In experiments with Al co-doped LYSO:Ce crystals, a Ce^{4+} related charge transfer (CT) band was observed in the absorption spectrum within the range of 200 nm to 350 nm.[15] This result suggests that Al ions indeed occupy the Si sites. However, our results suggest that the possibility of Al on Lu sites cannot be excluded, even though these defects are most probably benign defects that do not affect the optoelectronic properties given that they do not generate any gap states and defect transition levels.

4. Conclusion

The site occupation of Al doping in LSO crystals is significantly influenced by ionic radius and chemical valence. Our first-principles calculations revealed that Al doping favors Si sites under O-rich conditions and Lu sites under Si-rich conditions. Al favors low-coordinated Lu site, *i.e.*, the six-coordinated Lu_2 site, over the seven-coordinated Lu_1 site. Al on Si site introduces a shallow acceptor level, which could affect the electron trap and the ratio of Ce^{3+} and Ce^{4+}. Al on Lu site does not introduce any defect levels in the band gap. These results provide useful insights into the mechanisms of Al doping in LSO and theoretical support for further optimizing the doping strategies in LSO crystals.

Acknowledgements

Project supported by the National Key Research and Development Program of China (Grant No. 2022YFB3503900) and the National Natural Science Foundation of China (Grant No. 12305212).

References

[1] Melcher C and Schweitzer J 1992 *IEEE Trans. Nucl. Sci.* **39** 502
[2] Doshi N K, Shao Y, Silverman R W and Cherry S R 2000 *Med. Phys.* **27** 1535
[3] Lecoq P 2016 *Nuclear Instruments and Methods in Physics Research Section A: Accelerators, Spectrometers, Detectors and Associated Equipment* **809** 130
[4] Weber M J 2002 *Journal of Luminescence* **100** 35
[5] Di Francesco A, Bugalho R, Oliveira L, Pacher L, Rivetti A, Rolo M, Silva J, Silva R and Varela J 2016 *Journal of Instrumentation* **11** C03042
[6] Surti S and Karp J S 2016 *Physica Medica* **32** 12

[7] Melcher C, Koschan M, Zhuravleva M, Wu Y, Rothfuss H, Meng F, Tyagi M, Donnald S, Yang K, Hayward J *et al.* 2016 Scintillator design via codoping *Proceedings of International Symposium on Radiation Detectors and Their Uses* p. 020001

[8] Cooke D, Mcclellan K J, Bennett B L, Roper J, Whittaker M T, Muenchausen R E and Sze R 2000 *J. Appl. Phys.* **88** 7360

[9] Kimble T, Chou M and Chai B H 2002 Scintillation properties of LYSO crystals *IEEE Nuclear Science Symposium Conference Record*, Vol. 3 (IEEE) pp. 1434–1437

[10] Spurrier M A, Szupryczynski P, Yang K, Carey A A and Melcher C L 2008 *IEEE Trans. Nucl. Sci.* **55** 1178

[11] Blahuta S, Bessiere A, Viana B, Dorenbos P and Ouspenski V 2013 *IEEE Trans. Nucl. Sci.* **60** 3134

[12] Yang K, Melcher C L, Rack P D and Eriksson L A 2009 *IEEE Trans. Nucl. Sci.* **56** 2960

[13] Wu Y, Koschan M, Li Q, Greeley I and Melcher C L 2018 *Journal of Crystal Growth* **498** 362

[14] Cai J and Yeung Y y 2023 *Phys. Rev. B* **107** 085149

[15] Xue Z, Chen L, Zhao S, Yang F, An R, Wang L, Sun Y Y, Feng H and Ding D 2023 *Crystal Growth & Design* **23** 4562

[16] Syntfeld-Kazuch A, Moszynski M, Swiderski L, Szczesniak T, Nassalski A, Melcher C L and Spurrier M A 2008 Energy resolution of calcium co-doped LSO:Ce scintillators *IEEE Nuclear Science Symposium Conference Record* (IEEE) pp. 2744–2750

[17] Shannon R D 1976 *Foundations of Crystallography* **32** 751

[18] Kresse G and Furthmüller J 1996 *Comput. Mater. Sci.* **6** 15

[19] Blöchl P E 1994 *Phys. Rev. B* **50** 17953

[20] Kresse G and Joubert D 1999 *Phys. Rev. B* **59** 1758

[21] Perdew J P, Ruzsinszky A, Csonka G I, Vydrov O A, Scuseria G E, Constantin L A, Zhou X and Burke K 2008 *Phys. Rev. Lett.* **100** 136406

[22] Paier J, Marsman M, Hummer K, Kresse G, Gerber I C and Ángyán J G 2006 *J. Chem. Phys.* **124** 154709

[23] Freysoldt C, Grabowski B, Hickel T, Neugebauer J, Kresse G, Janotti A and Van de Walle C G 2014 *Rev. Mod. Phys.* **86** 253

[24] Zhang S and Northrup J E 1991 *Phys. Rev. Lett.* **67** 2339

[25] Freysoldt C, Grabowski B, Hickel T, Neugebauer J, Kresse G, Janotti A and Van de Walle C G 2014 *Rev. Mod. Phys.* **86** 253

[26] Lu L, Zhang H, Wu X, Shi J and Sun Y Y 2021 *Chin. Phys. B* **30** 096806

[27] Wu X, Ming C, Shi J, Wang H, West D, Zhang S and Sun Y Y 2022 *Chin. Phys. Lett.* **39** 046101

[28] Kobayashi M, Ishii M and Melcher C L 1993 *Nuclear Instruments and Methods in Physics Research Section A: Accelerators, Spectrometers, Detectors and Associated Equipment* **335** 509

[29] Kamenskikh I, Mikhailin V, Munro I, Petrovykh D, Shaw D, Studenikin P, Vasil'ev A, Zagumennyi I and Zavartsev Y D 1995 *Radiation Effects and Defects in Solids* **135** 391

[30] Lempicki A and Glodo J 1998 *Nuclear Instruments and Methods in Physics Research Section A: Accelerators, Spectrometers, Detectors and Associated Equipment* **416** 333

[31] Blahuta S, Bessière A, Viana B, Ouspenski V, Mattmann E, Lejay J and Gourier D 2011 *Materials* **4** 1224

[32] Ding D, Feng H, Ren G, Nikl M, Qin L, Pan S and Yang F 2010 *IEEE Trans. Nucl. Sci.* **57** 1272

[33] Melcher C L, Friedrich S, Cramer S P, Spurrier M A, Szupryczynski P and Nutt R 2005 *IEEE Trans. Nucl. Sci.* **52** 1809